Journal of Materials Chemistry A

Accepted Manuscript

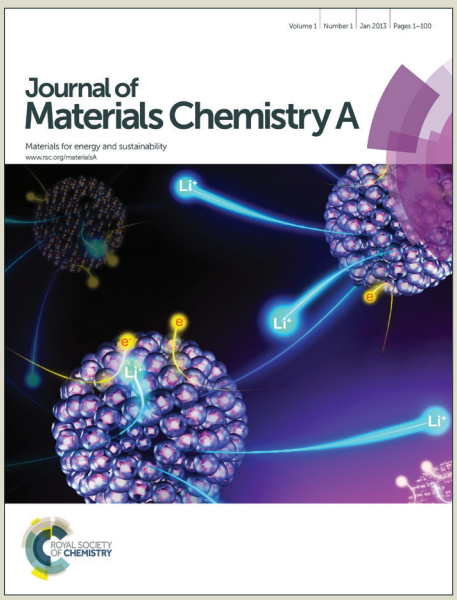

ROYAL SOCIETY OF CHEMISTRY

www.rsc.org/materialsA

Journal of Materials Chemistry

RSCPublishing

ARTICLE

Immobilization of iodine into a hydroxyapatite structure prepared by cementation

Cite this: DOI: 10.1039/x0xx00000x

Antoine Coulon,[a] Danielle Laurencin,[b] Agnès Grandjean,[c] Celine Cau Dit Coumes,[d] Sylvie Rossignol,[e] and Lionel Campayo,*[a]

Received 00th January 2012,
Accepted 00th January 2012

DOI: 10.1039/x0xx00000x

www.rsc.org/

In order to manage radioactive iodine-129 coming from nuclear spent fuel, robust host matrices with durable long term behaviour need to be developed. In this work, a new process of synthesis of an iodate-substituted hydroxyapatite by means of a cementation route is described. This material was obtained from a mixture of tetracalcium phosphate (TTCP), tricalcium phosphate (αTCP) and sodium iodate ($NaIO_3$), taken in a molar ratio 1/2/0.5. The progress of the reaction leading to the setting and hardening of cement paste was monitored by combined measurements of electrical conductivity and heat flux release, together with XRD characterizations of materials at definite times of hydration. Sodium iodate acts as a set retarder, by leading to the precipitation of non-cohesive transient phases, which are then destabilized when the massive precipitation of hydroxyapatite occurs. These delays can however be limited by adding hydroxyapatite seeds to the cement paste, which means that it is possible to control the setting time in view of an industrial application. This novel cementitious system leads to a porous material composed of iodine-substituted hydroxyapatite needles covering residual TTCP and αTCP particles. Iodine has mainly entered the hydroxyapatite structure under the form of iodate anions only. An iodine incorporation rate of 6.5 wt.% has been obtained by this cementitious system, which is a promising value in view of using these material for the conditioning of radioactive iodine.

Introduction

A common strategy for handling long-lived nuclear wastes consists in their disposal in a geological repository, after having immobilized them into robust inorganic matrices. For example, a series of borosilicate glasses have been developed by the French nuclear industry in order to immobilize most of the long-lived radionuclides (transuranic elements, fission products, fuel alloying elements and cladding elements) coming from spent nuclear fuel reprocessing.[1]

Iodine-129, one of the longest half-life radionuclides (15.7×10^6 years), cannot be immobilized in conventional borosilicate-based vitreous systems due to volatilization issues.[2] Thus, other methods are under investigation to develop specific matrices for iodine conditioning. For instance, immobilization of iodine as AgI or $Ba(IO_3)_2$ in a Portland cement-based material has already been investigated,[3] with iodine loadings ranging from 3 to 20 wt.%. Besides, the capacity of the different phases composing hydrated Portland cement to incorporate iodine by ionic exchange has also been studied. Among them, calcium silicate hydrate (C-S-H) seems to exhibit the highest capacity towards iodide or iodate retention,[4, 5] but the question of the chemical durability of a Portland cement-based matrix with respect to the half-life of iodine-129 is still considered as an issue.[6] This is why some low melting temperature glass matrices,[7, 8] calcium (sulfo)aluminate phases,[9-12] and also some ceramic matrices like iodine-bearing sodalite ($Na_8(AlSiO_4)_6I_2$) [13, 14] and iodine-bearing apatite[15-20] have been studied in order to incorporate iodine into the core of the materials. More recently, glass-bonded mordenite composites[21] and MOFs (Metal Organic Frameworks)[22-24] have also been proposed as possible matrices.

Among all these materials, apatite phases have focused our attention, because xenon-129, the decay product of iodine-129, was retained over geological time scales in the structure of apatite minerals ($\approx 4.56.10^9$ years old).[25] The iodide-bearing apatite with lead and vanadium ($Pb_{10}(VO_4)_{6-x}(PO_4)_xI_2$ with x=0 or 1.2) is the standard form[15, 16] for iodine-129 conditioning in apatites. It is obtained by reactive sintering from a stoichiometric mixture of lead phosphovanadate and lead iodide.[17] This matrix can incorporate a high iodine content (7 wt.%) and shows a good chemical durability.[18] Nevertheless, the complexity of its synthesis (pressure-assisted sintering techniques,[16, 17] microwave sintering[19]) and the use of toxic reactants can hinder their development at an industrial scale.

Fewer studies have been devoted to the incorporation of iodine under the form of iodate into confinement matrices, even though the lower mobility of iodates over iodides in the soil[26, 27] can be seen as a clear advantage. Our previous study had demonstrated the feasibility of obtaining an iodate-substituted hydroxyapatite powder by precipitation in water.[20, 28] This material, of general formula $Ca_{10}(PO_4)_6(OH)_{1.6}(IO_3)_{0.4}$, has the

advantage of being prepared without using any toxic reactants. However, during the precipitation, a fraction of iodate remains in the aqueous phase, which would consequently become a secondary waste. Thus, in order to avoid this drawback, we decided to investigate another synthetic method of this material, using a cementation route. Although the possibility of using hydroxyapatite-based cements for radio-iodate immobilization had already been suggested,[29] no evidence had been brought of the feasibility of this synthetic procedure nor of the actual incorporation of iodate in the apatite structure by such a route. Thus, in this manuscript, we describe the very first experimental investigation of an iodate-substituted hydroxyapatite elaborated by cementation. The evolution of this system during the early ages will first be presented, and then the effective incorporation of iodate into apatite structure will be discussed.

Experimental

Synthesis

Calcium phosphate cements are obtained by dissolution in water of a calcium phosphate with Ca/P<1.67 and a calcium phosphate with Ca/P>1.67, followed by apatite precipitation. Many cementitious systems are described in literature.[30, 31] The reaction between a tricalcium phosphate ($\alpha Ca_3(PO_4)_2$), noted αTCP, and a tetracalcium phosphate ($Ca_4(PO_4)_2O$ or hilgenstockite), noted TTCP, was here chosen because of its reasonable setting time and the insurance of achieving the formation of a stoichiometric hydroxyapatite.[31]

The pure crystallized α allotropic form of the tricalcium-phosphate (TCP) phase (monoclinic structure) was obtained at high temperature in two steps. First, the β allotropic form of TCP (rhombohedral structure) was synthesized by solid state reaction from a stoichiometric mixture of $CaCO_3$ (Alfa Aesar, Germany, 99% purity) and $CaHPO_4$ (Alfa Aesar, Germany, 98% purity). The mixture was heated at 1000°C for 15 hours under air.[32] The obtained powder was ground for 5 minutes in a zirconia bowl with a 20 Hz frequency using a Retsch MM200 mill. Then, it was calcined at 1300°C during 4 hours under air[33] to stabilize the αTCP phase (the βTCP ↔ αTCP allotropic transition is at 1120°C)[34] and was subsequently quenched in air. The purity of the obtained powder was checked by X-ray diffraction (XRD) analysis. No remaining traces of βTCP were detected on the diffractograms of the powder obtained in such conditions.

Pure crystalline TTCP powder was synthesized by solid state reaction from a stoichiometric mixture of $CaCO_3$ and $(NH_4)H_2PO_4$ (Prolabo, France, 97.5% purity). The mixture was heated at 1400°C for 12 hours under air.[35, 36] The purity of the obtained powder was checked by XRD analysis.

The standard hydroxyapatite cement paste (i.e. without iodate), hereafter called Ce-HA, was prepared by adding water into a mixture of TTCP and αTCP powders. The dry mixture was weighed beforehand in stoichiometric amounts according to equation (1).

$$Ca_4(PO_4)_2O + 2Ca_3(PO_4)_2 + x\ H_2O \rightarrow Ca_{10}(PO_4)_6(OH)_2 + (x-1)\ H_2O \quad (1)$$

It is worth noting that "x" depends on the liquid-to-solid ratio and an excess of water is generally used (for stoichiometric conditions "x" would be equal to 1). In this work, the water-to-solid ratio of 0.48 was used, which corresponds to an x value of 30. After weighing, the dry stoichiometric mixture of αTCP and TTCP powders was ground for 5 minutes with 20 Hz frequency in a zirconia bowl (using a Retsch MM200 mill). A median particle size of 22 µm was determined by a laser particle sizer (MALVERN Mastersizer). The specific surface area was 0.3 $m^2.g^{-1}$, as measured by nitrogen absorption analysis at 77 K (Gemini 2360 Micrometrics), and applying the BET method. After 5 minutes of mixing of the dry powder with demineralized water, the paste was cured at room temperature in sealed polypropylene boxes to prevent desiccation without specific control of relative humidity of the atmosphere.

The iodate-substituted hydroxyapatite cement paste, hereafter referred to as CeHA+$NaIO_3$, was obtained from a stoichiometric mixture of TTCP / αTCP / $NaIO_3$ powders with a molar ratio of 1/2/0.5. This molar ratio corresponds to the calcium, phosphorous and iodine concentrations found by chemical analysis for an iodate-substituted hydroxyapatite obtained by simple precipitation[20] (iodine content ~ 7 wt.%). $NaIO_3$ (Alfa Aesar, Germany, 99% purity) was added to the dry mixture of reactants before grinding. After grinding, the specific surface area of the powder was 0.4 $m^2.g^{-1}$, as measured by the BET method. The preparation of the cement paste and the aging of the cement paste were realized following the same procedure as CeHA.

Another iodate-substituted hydroxyapatite cement, hereafter referred to as CeHA+$NaIO_3$+10%G, was also prepared following a similar procedure as for CeHA+$NaIO_3$, except that 10 wt.% of seeds were also added to the dry mixture of reactants after grinding. These seeds corresponded to an iodate-substituted hydroxyapatite previously obtained by the precipitation route.[20]

In each case, cement reaction was stopped after fixed periods of time (depending on the type of cement), by immersing the paste into isopropanol and drying it in an anhydrous atmosphere at room temperature.

Characterizations

Structural and chemical characterization of the final materials

Elemental analyses were carried by ICP-AES for calcium, sodium and phosphorus and by thermogravimetry for iodine (see Table S1 and page S2 in the ESI†).

Crystalline phases were investigated by X-ray diffraction at room temperature with a Panalytical MPD Pro fitted with a copper anode using the Cu Kα radiation (Kα1=1.54056 Å) generated at 40 mA and 40 kV. The 2θ range between 10 and 70° was used, and this range was scanned with a 0.017° step. Diffractograms were analyzed using the EVA version 10.0 rev. 1 program (DIFFRACTplus, Bruker) and were post-treated to get proportions of the different phases and unit-cell parameters of apatitic phases (see Tables S2 and S3 in the ESI†).

Desorption tests were performed to determine the iodine fraction which was physisorbed (i.e., not incorporated in the crystalline structure of a given phase). One gram of a one-month-old CeHA+$NaIO_3$ was milled for 5 minutes on a Retsch MM200 mill in a zirconia bowl with a 20 Hz frequency. The specific surface area of the powder was 7.1 $m^2.g^{-1}$, as measured by the BET method. The resulting powder was dispersed in 200 mL of deionized water during 5 hours. This suspension was filtered and iodine concentration in the filtrate was determined using an iodide selective electrode (Thermo Scientific), after a quantitative reduction of iodate to iodide with ascorbic acid.[37]

Thermogravimetric Analyses (TGA) were performed on a

Setaram Setsys Evolution 16-18 apparatus. After milling, the cement powder was heat-treated at 10°C.min^{-1} up to 1000°C under neutral atmosphere. Released gases were analysed by a mass spectrometer gas detector (Hiden Analytical QGA).

Scanning electron microscopy (SEM) observations and Energy-dispersive X-ray spectroscopy (EDXS) analyses of the bulk materials were performed on a Philips, Xl30 W-TMP and a Zeiss Supra 55. High Resolution transmission electron microscopy (HRTEM) measurements were performed on a JEOL 2200F microscope, equipped with an EDS silicon drift detector (JED 2300T, Jeol).

Raman spectra were acquired on a Horiba Jobin LabRam Aramis spectrometer in the 100-1600 cm^{-1} range, using a 532 nm wavelength laser.

^{1}H solid state NMR experiments were performed on a Varian VNMRS 400 MHz (9.4 T) NMR spectrometer, using a 3.2 mm Varian T3 HXY MAS probe and spinning at 20 kHz. Single pulse MAS (magic angle spinning) experiments were carried out, using a 2.5 µs 90° pulse. A recycle delay of 4 to 16 s was used (after checking that it ensured full relaxation of all ^{1}H resonances in each sample). A total of 16 to 32 transients were recorded for each sample. ^{1}H chemical shifts were referenced externally to a home-made hydroxyapatite sample ($Ca_{10}(PO_4)_6(OH)_2$), at 0 ppm (used as a secondary reference).

^{23}Na solid state NMR and ^{1}H{^{23}Na} REDOR studies of a one-month-old CeHA+$NaIO_3$ (Na/Ca molar ratio of 0.05) were performed on a Varian VNMRS 600 MHz NMR spectrometer, using a 3.2 mm Varian T3 HXY MAS probe and spinning at 10 kHz. For the ^{23}Na MAS NMR spectra, single pulse experiments were carried out using a 1 µs pulse (corresponding to a 30° flip angle for the solid), and a recycle delay of 45 s. Spinal-64 ^{1}H decoupling (100 kHz RF) was applied during acquisition. A total of 28 to 144 transients were recorded, depending on the sample. ^{23}Na chemical shifts were referenced to external NaCl at 7.19 ppm (used as a secondary reference). For the ^{1}H{^{23}Na} REDOR (Rotational Echo Double Resonance) studies, ^{1}H π/2 and π pulses of 2.5 and 5 µs were used, and ^{23}Na recoupling π pulses of 6 µs (the duration of the ^{23}Na pulses was optimized directly on the sample). The recycle delay was set at 8 s, and the number of transients acquired ranged from 256 to 1024. The purpose of these experiments was to probe the spatial proximity between the Na^+ cations and the OH groups of the apatite structure. In addition to the cement pastes prepared here, the REDOR spectra of two reference apatite samples were also recorded in the same conditions: a Na^+-substituted hydroxyapatite (Na/Ca molar ratio of 0.12), hereafter called NaHA, and a cow tooth (Na/Ca molar ratio of 0.05), hereafter called CT.[38]

To complete our knowledge of elemental environments in the cement, X-Ray Absorption Near Edge Structure (XANES) characterizations were performed at the I L_3-edge at the Soleil Synchrotron (see page S4 in the ESI for experimental details†).

Time-resolved characterizations

Different methods can be used to follow the progress of reaction of a calcium phosphate cement. Because of the exothermicity of the reaction (exothermic dissolution of the reactants), the reaction leading to setting and hardening can be easily monitored by microcalorimetry.[39] This characterization method had already been used with success to characterize the reactivity of apatite cements.[39, 40] In the present study, we paid a particular attention to the time at which the heat flow reached its maximum. Comparing this parameter for the different investigated cementitious systems provided information on their reactivity.[40] The evolution of the heat flux was characterized using a highly sensitive Setaram C80-type microcalorimeter under isothermal conditions at 25 ± 0.5°C for 6 days. Measurements were recorded by comparing the heat flow from an experimental chamber containing 2 g of sample to the heat flow of an inert control chamber containing 2 g of alumina.

In order to complete the investigation of the evolution of apatite cements at early age, these measurements were compared to the evolution of the conductivity of the cement pastes. This kind of approach was successfully applied to Portland cement[41] and calcium sulfo-aluminate cement.[42] Conductivity usually increases rapidly immediately after mixing due to the dissolution of anhydrous cement phases. Then, the interaction between dissolved ions in the mixing solution leads to the precipitation of cement hydrates. The consumption of ions and the decrease in their mobility due to progressive structuring of the paste are responsible for a decrease in the conductivity, which is sharp when the massive precipitation of hydrates occurs. To our knowledge, this method has not yet been applied to apatitic cements. In our study, the conductivity evolution of the pastes was measured over 6 days. The conductimetric cell was cylindrically shaped with two annular stainless steel electrodes, an inner radius of 15 mm, and a total volume of 70 mL. It was thermostated by circulation of cooling water in a double envelope. It was connected to the EC channel of an electrochemistry meter (Consort C 861) with a BNC cable. A specific data acquisition software (Consort Dis Data) was used to collect conductivity measurements. The conductivity cell was calibrated using a 12.888 mS/cm standardized KCl solution at 25 °C.

Results and discussion

Evolution of the system at early age

Figure 1A compares the evolution of the heat flow and electrical conductivity of the CeHA+$NaIO_3$+10%G paste. In this case, the heat flow reached its maximum 32 hours after mixing (Fig. 1, point 'e'), and the conductivity began to decrease sharply. It was also qualitatively observed that setting of the material occurred. The times necessary to reach maximum heat flux and conductivity drop for the three cements studied (CeHA, CeHA+$NaIO_3$ and CeHA+$NaIO_3$+10%G) are reported in Table 1.

Table 1 Influence of cement composition on the times for maximum heat flow and conductivity drop.

Sample	Maximum of heat flux released (in h)	Begin of conductivity decrease (in h)
CeHA	7±2	-
CeHA+$NaIO_3$	72±2	70<x<74
CeHA+$NaIO_3$+10%G	32±2	30<x<34

In the case of CeHA (the reference material without iodate), the heat production was much more rapid (Table 1): the maximum heat flow was recorded 7 h only after mixing and the conductivity continually decreased during the six days of the experiment. CeHA+$NaIO_3$ mixing exhibited the slowest reaction, with a maximum heat flow at 72 h. It can be concluded from these

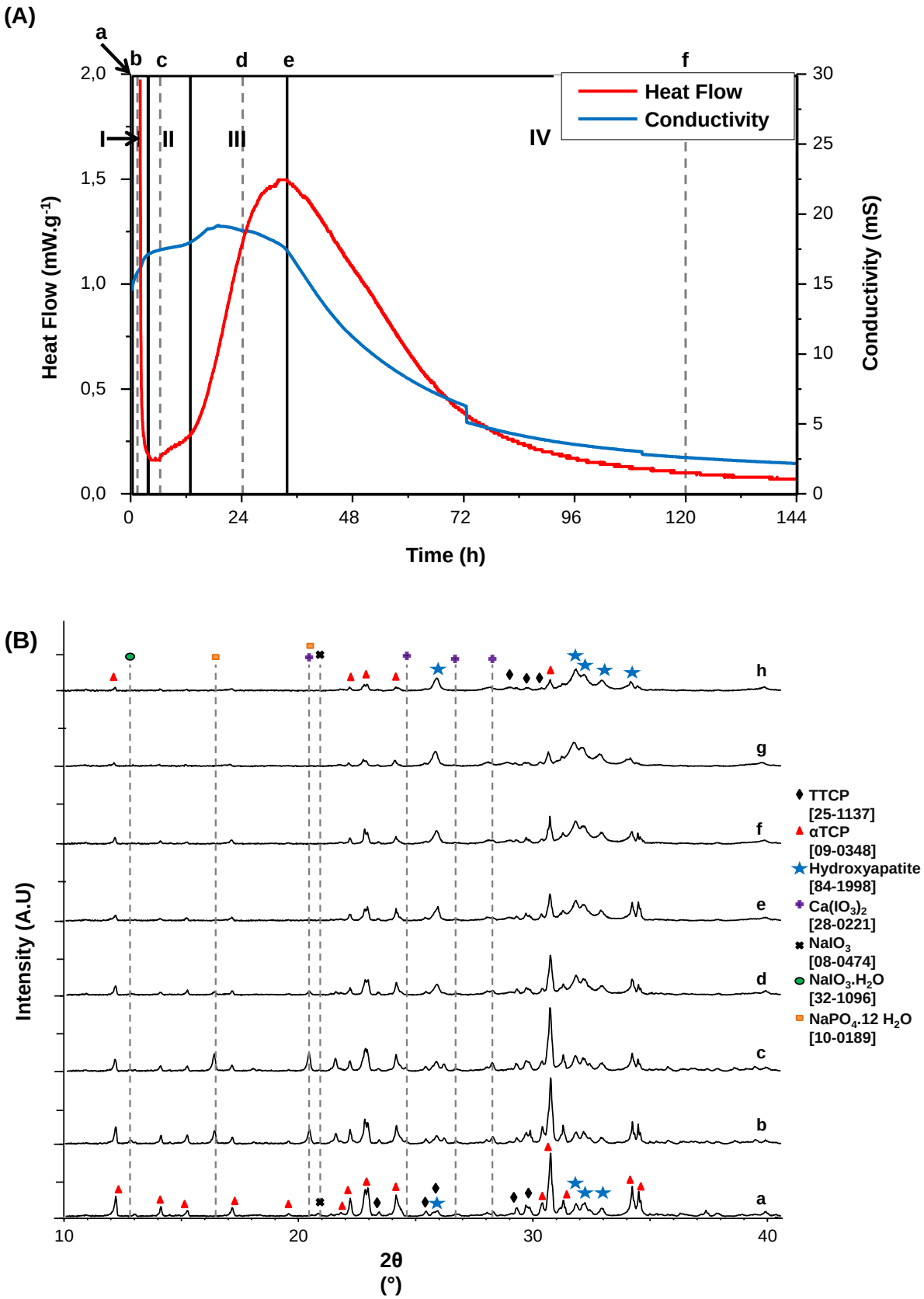

Fig. 1 (A) Microcalorimetric and conductivity curves of CeHA+$NaIO_3$+10%G during the first 6 days with the different hydration stops (from a to f) and the different steps (from I to IV). (**B**) XRD diagrams of CeHA+$NaIO_3$+10%G at different ages (a: dry powders, b: after 30 min of hydration, c: after 6 h of hydration, d: after 24 h of hydration, e: after 32 h of hydration, f: after 5 days of hydration, g: after 1 month of hydration, h: after 3 months of hydration)

observations that $NaIO_3$ is a set retarder of apatite cement. However, the delay could be reduced by addition of seeds (Table 1, CeHA+$NaIO_3$+10%G sample). Varying the amount of seeds might thus be a way to control cement setting for an industrial application.

CeHA+$NaIO_3$ and CeHA+$NaIO_3$+10%G differing only by the kinetics of phenomena, the second one was hereafter chosen to illustrate the evolution at early age, while the first was selected to probe iodine incorporation (avoiding possible interferences with seeds).

In order to identify the different stages occurring at early age, the evolution of the crystalline phases of the CeHA+$NaIO_3$+10%G system (Fig. 1B) was studied in addition to the microcalorimetry and conductivity analyses (Fig.1A). From the microcalorimetry and conductivity curves, the process was decomposed into four steps (Fig. 1A, sections I to IV), as detailed below.

It is worth noting that point 'a' on Fig. 1A corresponds to the mixture of reactants, before any water addition, and is considered as the reference. All the reactants are observed on the diffractogram (Fig. 1B, a) of the mixture of dry reactants.

The first step (section I on Fig. 1A), named the *starting period*, corresponds to the beginning of dissolution of reactants (αTCP, TTCP and sodium iodate). The dissolution of reactants provoked an increase of conductivity of the cement paste immediately after the addition of water. A first exothermic peak was also observed, resulting from various factors: wetting of anhydrous grains, dissolution of the reactants, germination of the first products, but also frictions occurring when the measurement cell was pushed down into the calorimetric chamber. The starting period occurred during the first five hours of hydration. It was characterized thanks to a cement sample for which hydration was stopped 30 minutes after mixing (point 'b' on Fig. 1A). At this step, two new crystalline phases were precipitated: $Ca(IO_3)_2$ and $Na_3PO_4.12H_2O$ (b on Fig. 1B). Another crystallized phase, characterized by a diffraction peak at 2θ=21.6°, was present, although we did not succeed in identifying it. Also, a $NaIO_3.H_2O$ phase, produced by the hydration of $NaIO_3$, was observed on this diffractogram.

After 6 hours, the conductivity was found to be stable, and the heat output was limited. This period is the *low thermal activity period* (section II on Fig. 1A), which continued until the 12th hour of hydration. During this period, a slight increase of the heat flux was observed. Crystallized phases present in the cement paste during this period were investigated with a cement sample for which the hydration was stopped 6 hours after mixing (point 'c' on Fig. 1A). All crystallized phases that composed the cement paste 30 min after the addition of water were still observed on diffractogram c (6 hours after the addition of water, Fig 1B.c). Nevertheless, a strong decrease in the intensity of the peaks associated to $NaIO_3.H_2O$ and $NaIO_3$ was noticed. Besides, the intensity of the peaks belonging to an apatite phase had slightly increased, highlighting the beginning of hydroxyapatite crystallization.

From the 12th to the 32nd hour after the addition of water, a sharp increase in the heat flux was noted. This step, represented by section III on Fig. 1A, is named *acceleration period*. The characteristic cement sample for this period was obtained by stopping the hydration after 24 hours (point 'd' on Fig. 1A). From this time of hydration onwards, the signatures of $NaIO_3.H_2O$ and $NaIO_3$ were not observed anymore by XRD (Fig. 1B, d). Furthermore, the intensity of the characteristic peaks of $Ca(IO_3)_2$, $Na_3PO_4.12H_2O$ and of the unknown phase have strongly decreased. This last observation reveals the progressive consumption of these phases. At the end of the acceleration period (Fig. 1B, e), these phases were no more present on the XRD diagrams, meaning that they were transient phases. In the same time, a significant increase in the intensity of the peaks characteristic of the apatite phase was observed, together with a drop of the amount of calcium orthophosphate reagent phases (namely, TTCP and αTCP).

Based on XRD, microcalorimetry and conductivity studies, the following sequence (leading to the maximum of the heat flux released) can be suggested to summarize these results:

i) Immediate hydration of the reactants; in particular, $NaIO_3$ is turned into $NaIO_3.H_2O$.

ii) Beginning of dissolution of the reactants: this causes the increase in conductivity during the starting period.

iii) Precipitation of $Ca(IO_3)_2$ and $Na_3PO_4.12H_2O$ (first hours): these crystalline phases are considered as transient phases and their precipitation initiates the plateau on the conductivity curve.

iv) Precipitation of apatite: the precipitation of this phase is indirectly responsible for the increase in the heat flow since it promotes the exothermic dissolution of the reactants. Moreover, it consumes phosphate and calcium ions, which tends to destabilize other calcium orthophosphates.

The fourth step of cementation, named *decelerating period*, is represented by section IV on Fig. 1A. The decelerating period was characterized by the decrease in the heat flow release and in the conductivity (Fig. 1A). These phenomena can be explained assuming a variation in the composition of the interstitial solution, but also most likely by the loss of mobility of the ionic species due to the structurization of the paste caused by setting. Six days after the beginning of mixing, a heat flux release was still observed, meaning that the cement paste is still under evolution. This phenomenon was confirmed by an increase in the apatite content detrimental to other calcium orthophosphates, as shown on the diffractogram of a cement sample for which the hydration was stopped 5 days after mixing (Fig. 1B, f). This slow evolution was observed until one month after mixing (Fig. 1B, g). However, even for such a time or longer times, traces of the orthophosphate reactants were still present on the XRD patterns (Fig. 1B, h).

A further analysis of the XRD diagram of a one-month-old CeHA+$NaIO_3$+10%G cement shows that it is composed of 73 wt.% of apatitic phase (see page S3 in the ESI†). This value does not significantly differ from the one obtained for a one-month-old CeHA+$NaIO_3$ cement (70 wt.%). In the latter case, unit-cell parameters of the apatitic phase (see page S3 in the ESI†) only reveal slight differences by comparison with $Ca_{10}(PO_4)_6(OH)_2$. This result was expected since iodate incorporation in the apatitic structure proceeds by a distorsion of local environment around this anion,[28] without any drastic change of unit-cell parameters.[20]

Characterization of the obtained iodo-apatitic cement

In order to prove the incorporation of iodine in the solid, and more specifically in the apatite structure, a series of additional

characterizations were performed on a one-month-old CeHA+$NaIO_3$ cement.

Iodine incorporation within the solid

First, a global elemental analysis of the as-synthesized cement was carried out. This analysis shows no significant difference between experimental concentrations and expected values (see page S2 in the ESI†).

Then, a desorption test was performed on the one-month-old CeHA+$NaIO_3$ sample to verify that iodine did not merely remain as a physisorbed species at the surface of particles. Within the uncertainty range of our measurement, no iodine was detected in solution after desorption, meaning that the amount of physisorbed iodine was below 1 wt.%, which is far beneath the initial content iodine in the cement.

A TGA analysis coupled with mass spectrometry (MS) gas analysis of the iodate-containing cement was performed (Fig. 2) to get an insight on the thermal stability of the material. Gas analysis during the heat treatment (Fig. 2) showed a beginning of iodine volatilization at 500°C, which is similar to what had been obtained for an iodate-substituted hydroxyapatite synthesized by precipitation (~550°C).[20] Iodine may volatilize under I_2O_5 form, which is decomposed into I_2 and O_2 in this temperature range.[43] TGA analysis showed a weight loss of 8.5 wt% between 500°C and 1000°C (Fig. 2), in agreement with the initial iodine loading of 6.5 wt.% (taking into account oxygen associated with iodine). This result thus suggested that all the iodine added in the dry mixture of reactants had been incorporated into the cement. Further characterizations were then performed to analyze its presence in the apatite structure, as detailed below.

Textural characterization

The texture of the one-month-old CeHA+$NaIO_3$ cement was observed by SEM and TEM. As expected, this cement was found to be a porous material composed of agglomerates, the size of which ranged between 1 and 100 µm (Fig. 3a). The surface of all observed agglomerates was composed of needles of less than 500 nm long (Fig. 3b and 3c), the acicular

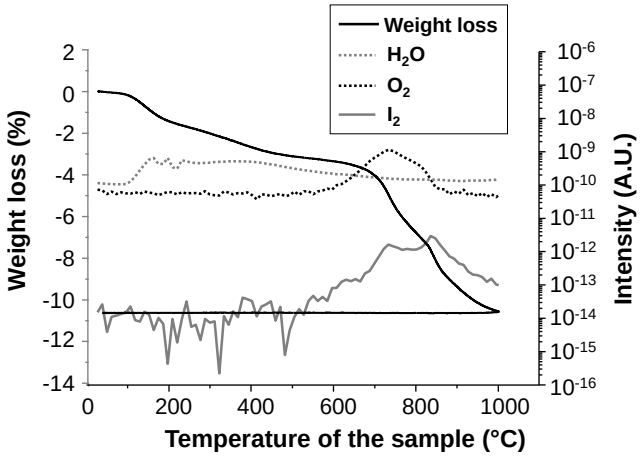

Fig. 2 TGA curve of CeHA+$NaIO_3$ after one month and MS analysis of released gases.

morphology of these needles being characteristic of apatite. It was found that the qualitative composition of the needles (analyzed on single needle by TEM coupled with EDX) included calcium, phosphorous and iodine. Specifically, the presence of iodine in the needles was attested by the presence of $L_{\beta1}$ (4.21 keV) and $L_{\beta2}$ (4.56 keV) transitions (see Figure S1 in the ESI†). Finally, it is worth noting that the size of the agglomerates corresponded to the typical grain size of the reactants. Thus, the presence of remaining traces of reactants at the center of the agglomerates cannot be excluded.

Iodine oxidation state determination

In order to determine the oxidation state of iodine, the Raman spectrum of a one-month-old CeHA+$NaIO_3$ sample was acquired and compared to an iodate-substituted hydroxyapatite obtained by wet precipitation (Fig. 4). No difference was observed between both Raman spectra. Vibration bands characteristic of apatitic phosphate groups[43-46] were identified on the Raman spectrum of the cement, and a broad band centered at 770 cm^{-1} was also visible, which is characteristic of the I-O stretching vibration in iodate ions.[47, 48] Moreover, no

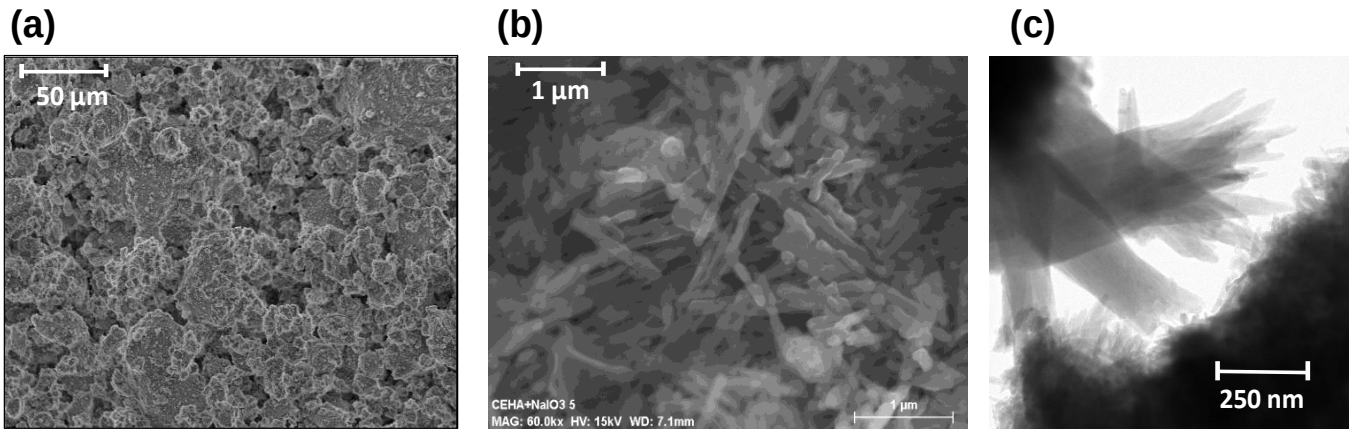

Fig. 3 Secondary electron SEM images (a and b) and TEM observation (c) of a one-month-old CeHA+$NaIO_3$ cement.

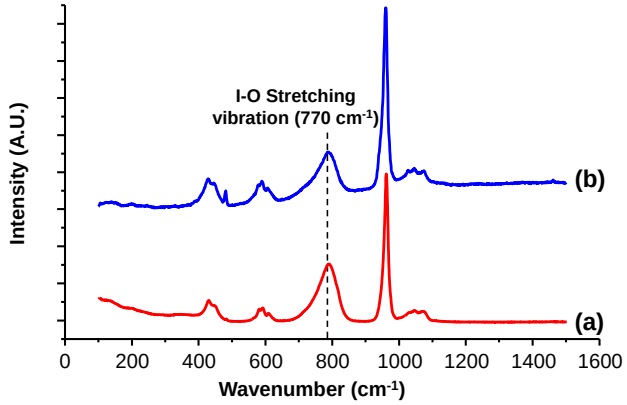

Fig. 4 Comparison Raman spectra between (a) an iodate-substituted hydroxyapatite prepared by wet precipitation route and (b) a one-month old cement paste of CeHA+$NaIO_3$.

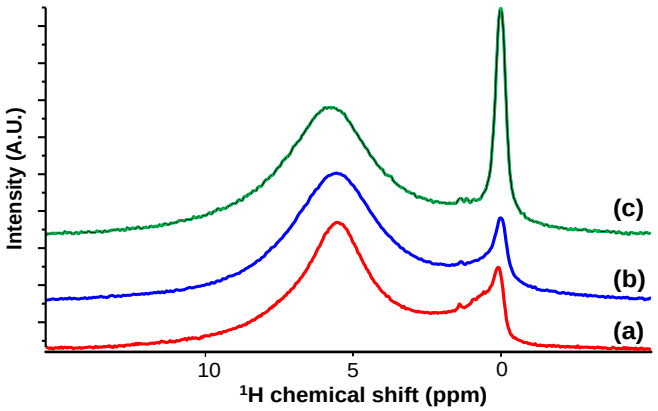

Fig. 5 ^{1}H-MAS-NMR of one month old samples CeHA+$NaIO_3$ (b) and CeHA (c) compared with an iodate-substituted hydroxyapatite prepared by wet precipitation (a).

band at 150-200 cm^{-1} corresponding to iodide-cation bonds was detected.[49] Thus, in the cement, iodine is only in the form of iodate.

Structural characterization

In order to further demonstrate the incorporation of the iodates into the apatitic structure, XANES and solid state NMR characterizations were performed.

The I L_3-edge XANES signatures of a one-month-old CeHA+$NaIO_3$ cement and that of an apatite obtained by wet precipitation according to the protocol described in reference 20 were compared (see Figure S2 in the ESI†). The two spectra are similar. Given that the apatite obtained by wet precipitation is composed of a unique phase, this suggests that the only environment met for iodine in the cementitious material is the same as for the precipitated powder, namely that of an apatitic structure. Moreover, the I L_3-edge XANES spectrum of the one-month-old CeHA+$NaIO_3$ cement was also recorded after having washed the material, in view of eliminating possible residual soluble phases (which may have contained iodate). The spectrum of the washed cement is the same as before washing, which further confirms that the iodate is in an apatite-like environment, and not in secondary (more soluble) phases. Consequently, no other phase has incorporated this element.

The ^{1}H solid state NMR spectrum of CeHA+$NaIO_3$ was compared to the ^{1}H solid state NMR spectra of CeHA (prepared without iodate) and of an iodate-substituted hydroxyapatite prepared by a precipitation route,[20] in order to confirm that the substitution scheme for the iodate was the same in both cases. In the case of iodate-substituted hydroxyapatites prepared by precipitation (Fig. 5a), it had been shown that IO_3^- incorporation leads to a decrease in the relative intensity of the OH^- peak on the ^{1}H solid state NMR spectra.[20] Such a decrease was also observed in the case of the cement pastes described here (Fig. 5b). However, several interpretations can be proposed for the decrease in intensity of the hydroxyl peak in the cement paste. Indeed, it is worth noting that traces of sodium were also detected on the EDXS spectra of the cement, which come from the $NaIO_3$ precursor. Na^+ is known for being able to substitute for Ca^{2+} in the apatite structure,[38] and to require a charge balance which can be achieved either by the simultaneous incorporation of CO_3^{2-} and/or creating vacancies on OH^- sites.[50-51] In the latter case, a decrease in intensity of the OH^- peak on the ^{1}H NMR spectra could consequently be due to sodium incorporation in the apatite structure, and not just to the substitution of the hydroxyls by iodates. Moreover, the presence of CO_3^{2-} and/or of HPO_4^{2-} anions[52] in the apatite structure can also result in a charge balancing scheme implying the creation of vacancies on OH^- sites. Thus, a correct interpretation of the underlying mechanism leading to iodate incorporation in the apatite cement required further verifications.

On the Raman spectrum of CeHA+$NaIO_3$, no bands corresponding to HPO_4^{2-} or CO_3^{2-} were observed: the ν_1 (P-O) vibration band at 1000 cm^{-1} of HPO_4^{2-} [44], the ν_4 (C-O) vibration band of CO_3^{2-} at 675 cm^{-1} and the ν_1 (C-O) vibration band of CO_3^{2-} at 1072 cm^{-1} [46, 50] were absent (Fig. 4). This means that in addition of the presence of iodate, only the presence of sodium may have been responsible for the decrease in the OH^- peak on ^{1}H solid state NMR spectra. In order to determine whether Na^+ was indeed incorporated inside the HA structure or not, ^{23}Na MAS NMR and ^{1}H{^{23}Na} REDOR analyses were carried out.

Despite the low concentration of sodium in CeHA+$NaIO_3$, a ^{23}Na MAS NMR was obtained in reasonable experimental time (~30 min). The ^{23}Na resonance was centered between 2 and 3 ppm, and the ^{23}Na NMR lineshape was similar to the one recorded for two reference samples: a Na-substituted HA phase (NaHA) and a cow tooth (CT) (Fig. 6a). For both of these reference samples, it had been demonstrated that Na^+ is located inside the HA structure, in close vicinity to the OH^- groups.[38] Thus, based on the simple comparison of the ^{23}Na MAS NMR spectra, it was tempting to speculate that Na^+ is also located inside the apatite structure in CeHA+$NaIO_3$. However, additional ^{1}H{^{23}Na} REDOR experiments were carried out to test this hypothesis.

The purpose of ^{1}H{^{23}Na} REDOR experiments was to probe the spatial proximity between the Na^+ cations and the OH^- groups of the apatite structure, using the ^{1}H-^{23}Na dipolar

coupling. In the REDOR experiment, two spectra are successively recorded, without (S_0) or with (S) ^{23}Na recoupling pulses. If the ^{1}H hydroxyl signal decreases in intensity in the "S" spectrum, this means that the apatitic OH groups are in close proximity to Na^+, and thus that sodium is incorporated into apatite structure. This is well illustrated in the cases of NaHA and CT, where an overall decrease in intensity of the ^{1}H signal was observed in the presence of ^{23}Na recoupling pulses (Fig. 6b). In contrast, in the case of the one-month-old CeHA+$NaIO_3$, with a similar Na content as in the NaHA and CT samples, no change in intensity of the hydroxyl peak between S and S_0 was observed, thereby demonstrating that Na^+ was actually *not* incorporated into the apatitic structure in the cement. Thus, it can be assumed that sodium has been incorporated into an amorphous phase, which has not been identified so far.

All in all, based on these additional solid state NMR experiments, the decrease in intensity of the ^{1}H signal in the case of the CeHA+$NaIO_3$ sample (Fig. 5b) was unambiguously ascribed to the incorporation of iodates inside the apatite structure, by substitution of the hydroxyls. Thus, the incorporation mechanism of iodates into the apatitic cement seems to be similar to the incorporation of iodate into a hydroxyapatite phase elaborated by the precipitation route.[20]

Based on the amount of apatite present in a one-month-old CeHA+$NaIO_3$ cement (~ 70 wt.%, as determined by a quantitative analysis of X-Ray powder diffraction data (see Table S2 in the ESI†)), and given the fact that apatite is the only phase to incorporate iodine, this would result in an apatite containing around 9.3 wt.% of iodine. Namely, for a stoichiometric apatite with a substitution of hydroxyl groups by iodate anions, this would lead to the following formula: $Ca_{10}(PO_4)_6(IO_3)_{0.83}(OH)_{1.17}$.

Conclusion

A cementation route was here examined to obtain a monolith of hydroxyapatite incorporating iodine in its structure with the objective of producing a potential host matrix to immobilize radio-iodine. It was demonstrated for the first time that such a material can be obtained starting from an αTCP, TTCP and sodium iodate mixture. The reactivity of this system was followed by microcalorimetry, conductivity measurements and XRD characterizations which showed an evolution towards hydroxyapatite through intermediate phases like calcium iodate *in a reasonable time.* Actually, sodium iodate was found to act as a set retarder, but the resulting delay could be modulated thanks to the addition of seeds giving a setting time comprised between 32 and 72 hours. After one month, the bulk material was composed of traces of the orthophosphate reactants and of a dominant apatite phase. A detailed structural investigation of this newly formed apatite by solid state NMR techniques, I L_3-edge XANES and Raman spectroscopy highlighted the fact that iodine was only incorporated under the form of iodate in the apatitic structure. The underlying mechanism involved a substitution of hydroxyl groups by iodate ions, a similar mechanism to wet precipitation route, but without the drawback of the generation of secondary wastes. All in all, this route to iodine-containing apatitic cements is particularly promising for the conditioning of radio-active iodine, with minimal secondary waste.

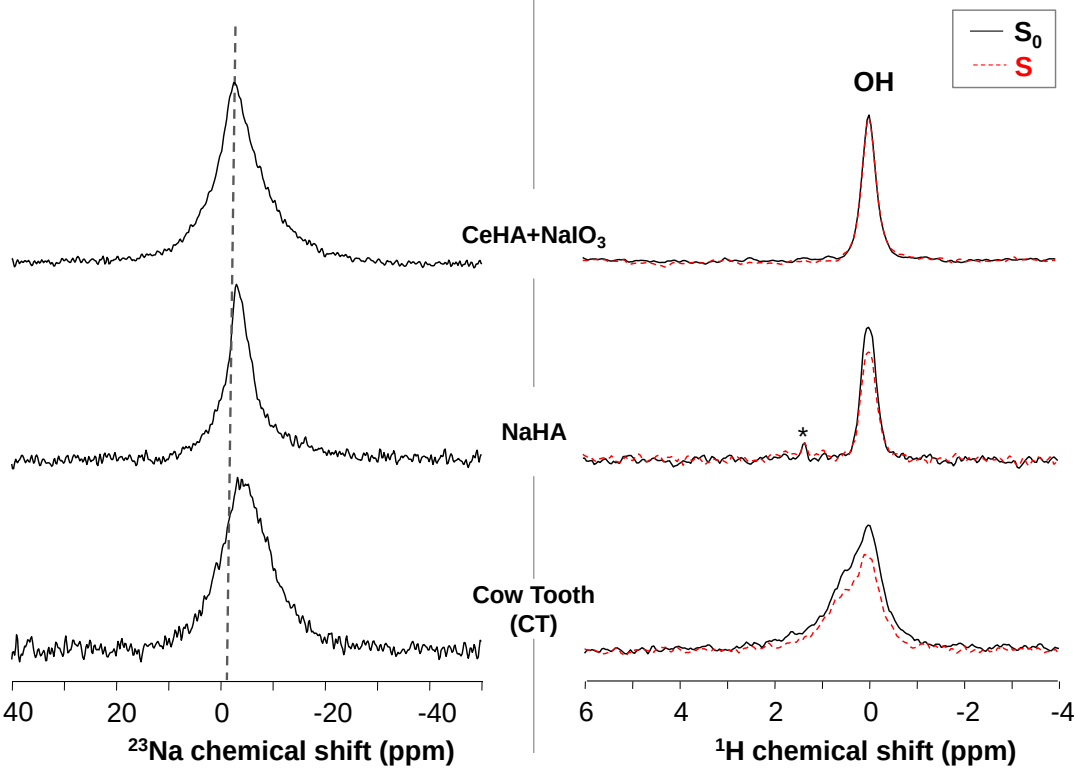

Fig. 6 (a) ^{23}Na MAS NMR and (b) ^{1}H{^{23}Na} REDOR spectra (spin-echo control spectrum S_0 and REDOR spectrum S) of NaHA, CT and CeHA+$NaIO_3$.

Acknowledgements

CEA and CNRS are acknowledged for financial support. We would like to thank Pascal Antonucci (CEA Marcoule, LP2C) for his help for microcalorimetry and conductivity experiments, Virginie Fremy (CEA Marcoule, LPSD) for elemental analyses and Nicolas Massoni (CEA Marcoule, LDMC) for structural developments by XRD. The authors would also like to thank the European Community and region of Languedoc Roussillon for the funding TEM/EDXS apparati, and Franck Godiard (from the electron microscopy service of the University of Montpellier II), and Xavier LeGoff (from ICSM, Marcoule) are acknowledged for their help with these characterizations. We acknowledge the French synchrotron SOLEIL for provision of synchrotron radiation facilities (project 20140494), and Delphine Vantelon from the LUCIA beamline for her assistance in the experiments.

Notes and references

[a] CEA, DEN, DTCD, SECM, Laboratoire d'étude et de Développement de Matrices de Conditionnement, Centre de Marcoule, 30207 Bagnols sur Cèze, France.

[b] Institut Charles Gerhardt Montpellier ICGM, UMR 5253 CNRS-UM2-UM1-ENSCM, Université de Montpellier 2, Place E. Bataillon, CC1701, 34095 Montpellier Cedex 5, France.

[c] Institut de Chimie Séparative de Marcoule, ICSM, UMR5257 CEA-CNRS-UM2-ENSCM, 30207 Bagnols sur Cèze, France.

[d] CEA, DEN, DTCD, SPDE, Laboratoire de Physico-Chimie des matériaux Cimentaires, Centre de Marcoule, 30207 Bagnols sur Cèze, France.

[e] Groupe d'Etude des Matériaux Hétérogènes, CEC-GEMH-ENSCI, 12 rue de l'Atlantis, 87068 Limoges Cedex, France.

† Electronic supplementary information (ESI) available: elemental analysis of a one-month-old CeHA+$NaIO_3$ cement (p. S2), quantitative analysis of the X-Ray powder diffraction data and unit cell parameters of apatitic phases (p. S3), I L_3-edge XANES characterizations (p. S4), TEM/EDXS analysis of a one-month-old CeHA+$NaIO_3$ cement (Figure S1), I L_3-edge XANES spectra of a one-month-old CeHA+$NaIO_3$ cement (before and after washing) and of a wet precipitated iodate-bearing apatite (Figure S2).

1. I. W. Donald, B. L. Metcalfe and R. N. J. Taylor, *J. Mater. Sci.* 1997, **32**, 5851-5887.
2. J.G. Darab, E.M. Meiers, and P.A. Smith, *Materials Research Society Symposium - Proceedings*, 1999, **556**, 215-222)
3. W.E. Clark, *Trans. Am. Nucl. Soc.* 1976, **23,** 264-265.
4. M. Atkins and F. P. Glasser, *Waste Manage.* 1992, **12**, 105-131.
5. I. Bonhoure, A. M. Scheidegger, E. Wieland and R. Dahn, *Radiochim. Acta*, 2002, **90**, 647-651.
6. R. D. Scheele, L. L. Burger and K. D. Wiemers, *ACS Sym. Ser.* 1984, **246**, 373-387.
7. H. Fujihara, T. Murase, T. Nishi, K. Noshita, T. Yoshida and M. Matsuda, *Materials Research Society Symposium - Proceedings*, 1999, **556**, 375-382.

8. T. Sakuragi, T. Nishimura, Y. Nasu, H. Asano, K. Hoshino and K. Iino, *Materials Research Society Symposium - Proceedings*, 2008, **1107**, 179-286.
9. M. Toyohara, M. Kaneko, N. Mitsutsuka, H. Fujihara, N. Saito and T. Murase, *J. Nucl. Sci. Technol*. 2002, **39**, 950-956.
10. D. R. Brown and M. W. Grutzeck, *Cement Concrete Res.* 1985, **15**, 1068-1078.
11. J. P. Rapin, A. Walcarius, G. Lefevre and M. Francois, *Acta Crystallogr. C*, 1999, **55**, 1957-1959.
12. L. Aimoz, D. A. Kulik, E. Wieland, E. Curti, B. Lothenbach and U. Mader, *Appl. Geochem.* 2012, **27**, 2117-2129.
13. D. M. Strachan and H. Babad, *Am. Ceram. Soc. Bull.* 1979, **58**, 327-327.
14. D. Hirabayashi, Y. Tanada, T. Sugiyama, Y. Enokida and K. Sawada, *AIChE J*. 2012, **58**, 2441-2447.
15. F. Audubert, J. Carpena, J. L. Lacout and F. Tetard, *Solid State Ionics*, 1997, **95**, 113-119.
16. L. Campayo, S. Le Gallet, Y. Grin, E. Courtois, F. Bernard and F. Bart, *J. Eur. Ceram. Soc.* 2009, **29**, 1477-1484.
17. S. Le Gallet, L. Campayo, E. Courtois, S. Hoffmann, Y. Grin, F. Bernard and F. Bart, *J. Nucl. Mater*. 2010, **400**, 251-256.
18. C. Guy, F. Audubert, J. E. Lartigue, C. Latrille, T. Advocat and C. Fillet, *C. R. Phys.* 2002, **3**, 827-837.
19. M. C. Stennett, I. J. Pinnock and N. C. Hyatt, *J. Nucl. Mater.*, 2011, **414**, 352-359.
20. L. Campayo, A. Grandjean, A. Coulon, R. Delorme, D. Vantelon and D. Laurencin, *J. Mater. Chem.* 2011, **21**, 17609-17611.
21. T. J. Garino, T. M. Nenoff, J. L. Krumhansl and D. X. Rademacher, *J. Am. Ceram. Soc*. 2011, **94**, 2412-2419.
22. D. F. Sava, M. A. Rodriguez, K. W. Chapman, P. J. Chupas, J. A. Greathouse, P. S. Crozier and T. M. Nenoff, *J. Am. Chem. Soc.* 2011, **133**, 12398-12401.
23. K. W. Chapman, D. F. Sava, G. J. Halder, P. J. Chupas and T. M. Nenoff, *J. Am. Chem. Soc*. 2011, **133**, 18583-18585.
24. D. F. Sava, K. W. Chapman, M. A. Rodriguez, J. A. Greathouse, P. S. Crozier, H. Y. Zhao, P. J. Chupas and T. M. Nenoff, *Chem. Mater*. 2013, **25**, 2591-2596.
25. R. H. Nichols, C. M. Hohenberg, K. Kehm, Y. Kim and K. Marti, *Geochim. Cosmochim. Ac*. 1994, **58**, 2553-2561.
26. M. Fukui, Y. Fujikawa and N. Satta, *J. Environ. Radioactiv*. 1996, **31**, 199-216.
27. M. Fuhrmann, S. Bajt and M. A. A. Schoonen, *Appl. Geochem.* 1998, **13**, 127-141.
28. D. Laurencin, D. Vantelon, V. Briois, C. Gervais, A. Coulon, A. Grandjean and L. Campayo, *RSC Advances*, 2014, **4**, 14700-14707.
29. P. W. Brown, US Patent 5678233, 1999.
30. S. V. Dorozhkin, *Materials*, 2009, **2**, 221-291.
31. Y. Fujishiro, Y. Mizutani, S. Uchida and T. Sato, *Brit. Ceram. T.* 1999, **98**, 141-145.
32. M. Yashima, A. Sakai, T. Kamiyama, A. Hoshikawa, *J. Solid Sate Chem.* 2003, **175**, 272-277.
33. C. L. Camire, U. Gbureck, W. Hirsiger and M. Bohner, *Biomaterials*, 2005, **26**, 2787-2794.
34. H. Margot-Marette and P.V. Ribout, *Mem. Sci. Rev. Metall.* 1966, **63**, 959-967
35. C. Moseke and U. Gbureck, *Acta Biomater*. 2010, **6**, 3815-3823.
36. Y. Sargin, M. Kizilyalli, C. Telli and H. Guler, *J. Eur. Ceram. Soc.* 1997, **17**, 963-970.
37. G.S. Deshumukh, M.G. Bapat, *Fresen Z Anal Chem.*. 1955, **147**, 271-273.
38. D. Laurencin, A. Wong, W. Chrzanowski, J. C. Knowles, D. Qiu, D. M. Pickup, R. J. Newport, Z. H. Gan, M. J. Duer and M. E. Smith, *Phys. Chem. Chem. Phys.* 2010, **12**, 1081-1091.
39. C. S. Liu, H. F. Shao, F. Y. Chen and H. Y. Zheng, *Biomaterials*, 2003, **24**, 4103-4113.
40. C.L. Camire, U. Gbureck, W. Hirsiger, M., Bohner, *Biomaterials*, 2005, **26**, 2787-2794.
41. G. Levida, A. Marchetti, G. Gallone, A. Princigallo, G.L. Guerrini *Cement Concrete Res*. 2000, **230**, 923-930.
42. J. B. Champenois, C. C. D. Coumes, A. Poulesquen, P. Le Bescop and D. Damidot, *Rheol. Acta*, 2013, **52**, 177-187.
43. C. Farley and M. Pantoya, *Journal of Thermal Analysis and Calorimetry- Proceeding.* 2010, **102**, 609-613.
44. G. Penel, G. Leroy, C. Rey and E. Bres, *Calcif. Tissue Int.* 1998, **63**, 475-481.
45. G. Penel, G. Leroy, C. Rey, B. Sombret, J. P. Huvenne and E. Bres, *J. Mater. Sci.-Mater. Med.* 1997, **8**, 271-276.
46. A. Antonakos, E. Liarokapis and T. Leventouri, *Biomaterials*, 2007, **28**, 3043-3054.
47. Balichev.T.G and G. A. Petrova, *Zh. Strukt. Khim.* 1973, **14**, 463-470.
48. J.R. Durig, O.D. Bonner and W.H. Breazeal *J Phys. Chem.1965*, **69**, 3886-3892.
49. K. Nakamoto, *Infrared and Raman Spectra of Inorganic and Coordination Compounds.*, Wiley Interscience Publication, 1986.
50. H.E. Mason, A. Kozlowski and B.L. Philips, *Chem. Mater.* 2008, **20**, 294-302.
51. M. E. Fleet and X. Liu, *Biomaterials*, 2007, **28**, 916-926.
52. Y. M. Pan and M. E. Fleet, in *Phosphates: Geochemical, Geobiological, and Materials Importance*, eds. M. J. Kohn, J. Rakovan and J. M. Hughes, 2002, pp. 13-49.